EXPERIMENTAL INVESTIGATION ON THE TENSILE PROPERTIES OF WEAKLY CEMENTED SANDSTONE IN CHINA SHENDONG MINING AREA

by

Peng LI[a,b,c], Zhi-Hu LI[a], Bin LIU[a*], Teng TENG[a,d], and Jun-Ting GUO[c]

[a] School of Energy and Mining Engineering, China University of Mining and Technology, Beijing, China
[b] Shenhua Shendong Coal Group Company Limited, Shenmu, China
[c] State Key Laboratory of Water Resource Protection and Utilization in Coal Mining, Beijing, China
[d] State Key Laboratory of Coal and CBM Co-mining, Jincheng, China

Original scientific paper
https://doi.org/10.2298/TSCI2006987L

To investigate the tensile properties of weakly cemented rock samples at Shendong Mining Area. Four common weakly cemented rocks are subjected to Brazilian Splitting Test, and both the acoustic emission signals and deformation field are monitored simultaneously. Thus, deformation and acoustic emission features were analyzed in different rock samples. Moreover, the relationship between the evolution of localization belt and acoustic emission features was identified. The results show that the samples displayed similar deformation features and that the evolution of R value is also basically consistent.

Key words: *weakly cemented rock, Brazilian Splitting Test, acoustic emission, deformation field, R value*

Introduction

At present, a number of super-large coal mines with 10 million tons of annual capacity are being built in Shendong Mining Area. However, coal seams in this mining area generally have shallow enrichment, thin bedrocks and low cementation degree, which add to the difficulty of mining engineering and the risks of dynamic disasters. Thus, studying the tensile features of weakly cemented rock samples from Shendong Mining Area is of high importance.

Many researches have done a series of works on the weakly cemented strata in mining areas of Western China. Li *et al.* [1, 2] and Wang *et al.* [3] investigated the physical, mechanical features and the failure mode of weakly cemented rocks under uniaxial and triaxial compression process. Wang *et al.* [4] and Sanborn *et al.* [5] carried out many dynamic Brazilian tests of Geo-materials to analyze the deformation features. Yang *et al.* [6] and Suchorzewski *et al.* [7] discussed numerical investigations of rock behaviors during quasi-static splitting tension. Aliabadian *et al.* [8] conducted researches about the crack propagation features and deformation field evolution. The research related to bedding effect and anisotropy has been investigated, including the influencing mechanism of bedding angle, spatial distribution, and value changes of acoustic emission (AE) activity [9-11]. Digital image correlation (DIC) has been widely applied to strain measurement of rocks during the failure process due to the progress made in

* Corresponding author, e-mail: liubin@student.cumtb.edu.cn

high-speed camera [12, 13]. The AE characteristics during the loading process of coal or rock in different loaded ways were studied [14, 15].

However, the aforementioned studies are more concerned with the mechanical properties of weakly cemented strata under compressive load, but few studies have been conducted on the tensile properties and AE features of weakly cemented rocks. The aim of the present paper is to study the tensile properties of four kinds of weakly cemented rocks by using AE monitoring and high-speed strain measurement system in Brazilian Splitting Tests. Moreover, DIC is applied to the understanding of evolution of tension-induced displacement in localization belt in the deformation field. The relationship between the evolution of localization belt and AE features is identified. The research findings provide guidance for predicting dynamic disasters in weakly cemented rock strata in Shendong Mining Area.

Arrangements of experiment process

Sample preparation and experimental equipment

The rock samples were collected by geological drilling in No. 3 District of Buertai Coal Mine in Shendong Mining Area and sharped into standard Brazilian disc samples (∅50 mm × × 25 mm). The computer controlled electronic universal testing machine (Model: WDW-100E), AE monitoring system (Model: PCI-Express 8) and high-speed strain measurement system were used for the Brazilian Splitting Test, as seen in fig. 1).

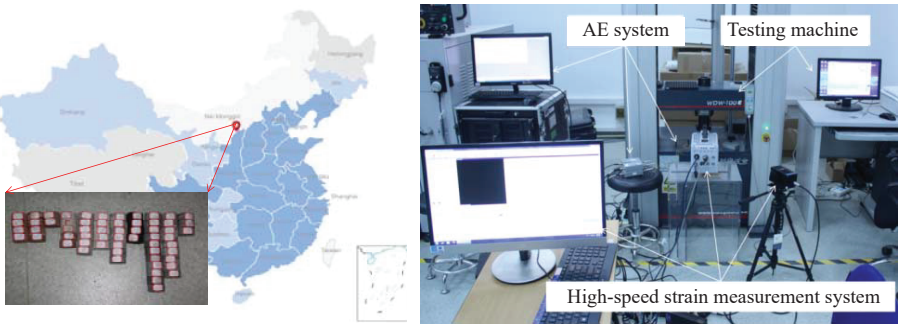

Figure 1. Sample preparation and the experimental equipment

Experimental scheme

Different rock samples were subjected to Brazilian Splitting Test with displacement-controlled loading under a loading rate of 0.20 mm per minute. AE signals and speckle images were collected and stored simultaneously during the loading process. Four AE sensors were installed to the back of the rock samples as designed (seen in fig. 2), and the front side was reserved for speckle image collection. The AE signal threshold was set to 45 dB, and the sampling rate was 1 MHz. Breaking lead test was performed after wiring, and it was ensured that a large amount of valid AE signals were acquired during the test. The sampling frequency was set to 50 Hz in the high-speed strain measurement system. Before the test, the front side of the rock samples was sprayed. Artificial speckle field was produced while ensuring that the high-speed camera could recognize the speckles on the sample surface, so that the deformation field on the sample surface could be acquired.

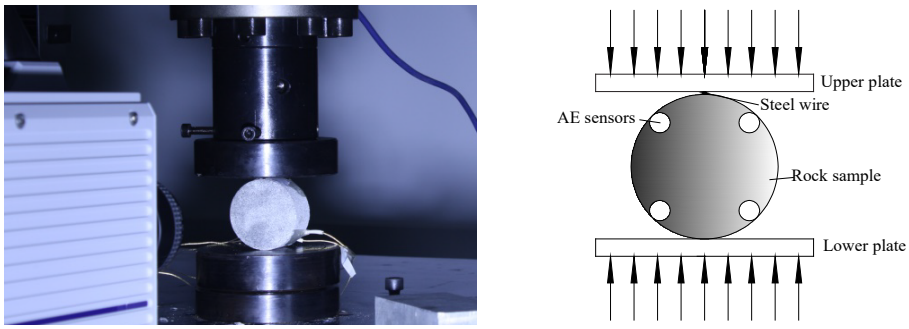

Figure 2. Loading under Brazilian splitting test

Results and discussion

Analysis of splitting failure features of weakly cemented rock samples

Table 1 lists the testing results of Brazilian splitting test. Figure 3 shows the stress-strain curves for representative samples for each of the four types. It is easy to find that the four types of rock samples have similar deformation features, but these features are different. Stress shows a near-linear increase in the yield stage and the failure stage is short. That is because the tensile strength of the minerals inside the rocks is far lower than its compressive strength. After the tensile stress reached the level of tensile strength, cracks develop rapidly until sample failure. Therefore, the deformation process can be divided into four stages, named compaction stage, elastic stage, post-elastic stage and failure stage, respectively.

Table 1. Physical and mechanical parameters of rock samples

Lithology	Sample no.	Failure load [kN]	Tensile strength [MPa]	Mean [MPa]
Sandy mudstone	021	3.04	1.55	1.76
	022	3.20	1.63	
	023	4.59	2.34	
	024	3.01	1.53	
Medium sandstone	411	3.28	1.67	1.39
	413	3.30	1.68	
	414	1.62	0.83	
Siltstone	511	4.08	2.08	1.71
	512	2.27	1.16	
	516	4.80	2.45	
	517	2.28	1.16	
Fine sandstone	531	4.02	2.05	1.67
	532	3.02	1.54	
	534	2.81	1.43	

Figure 3 also indicates that there are considerable differences in tensile strength and damage-induced deformation among the rock samples. The maximum mean tensile strength of the sandy mudstone is 1.76 MPa, and the minimum of the medium sandstone is 1.39 MPa. The maximum deformation of the medium sandstone is 1.06×10^{-2}, and the minimum was 6.98×10^{-3} in the siltstone. This is mainly due to the varying particle size of the rock samples: siltstone has the smallest particle size, fewest voids and most compact structure, which

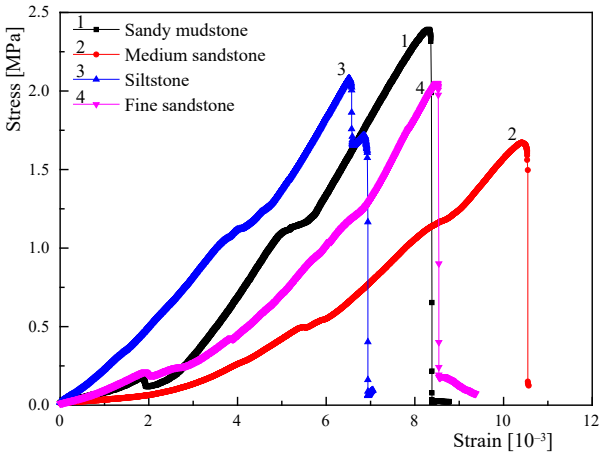

Figure 3. Stress-strain curves of representative rock samples

explains its minimum deformation. Sandy mudstone and fine sandstone comes next, and the particle size is the largest in medium sandstone, so the deformation is also the largest.

Thermal infrared analysis of rock fracture

Figure 4 is the abnormal infrared thermal imaging sequence of different kinds of sandstone samples at the failure moment. The high temperature around the cracks reflects that rock fracture is an exothermic process. From fig. 4, one can find that the energy dissipated during the failure of medium sandstone is small due to the large particle size, indicating that the dynamic phenomenon is not obvious. Under the action of external disturbance, most of the energy of siltstone is used for the failure of the rock mass. Therefore, the specimens are crushed.

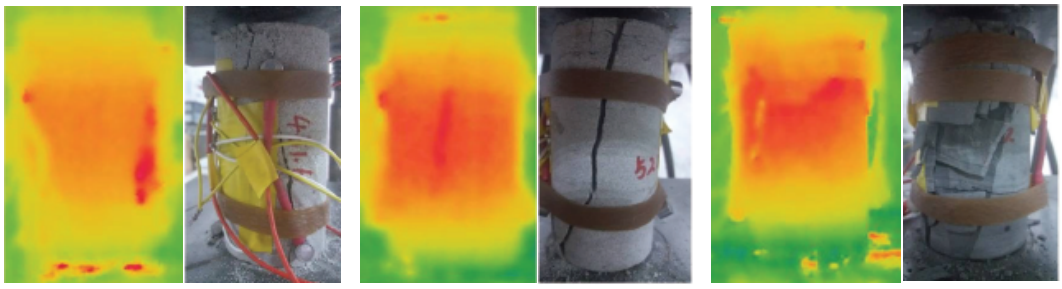

(a) (b) (c)

Figure 4. Abnormal infrared thermal imaging of different kinds of sandstone at the failure moment; (a) medium sandstone, (b) siltstone, and (c) fine sandstone

Displacement evolution of localization belt in weakly cemented rocks

In order to analyze the displacement evolution of the localization belt in different rocks during the loading process, the speckle images at the start of loading were taken to obtain the deformation field. Figure 5 shows the failure mode and deformation field just before the moment of rupture in representative samples for the four types of rocks. Apparently, the failure morphology of rock samples is in complete agreement with the localized deformation field. The sites of rock rupture are basically parallel with the loading direction, and the rupture plane passes through the center of disc. Due to structural differences in some samples, the rupture plane does not pass through the center of disc. Compared with siltstone sample 516 and sandy mudstone sample 022, cracks in the fine sandstone sample 531 and medium sandstone sample 411 are more obvious, indicating more violent rupture.

Three groups of measuring points (P1, P2, P3) were arranged on the two sides of the localization belt to analyze the displacement evolution. The measuring points were laid

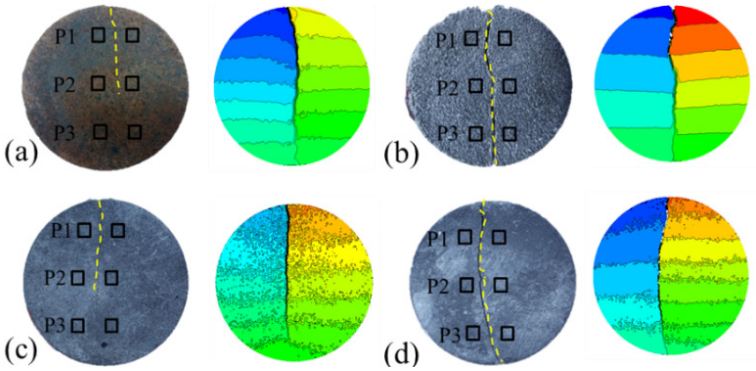

Figure 5. Failure mode and deformation field before rupture for representative rock samples; (a) sandy mudstone sample 022, (b) medium sandstone sample 411, (c) siltstone sample 516, and (d) fine sandstone sample 531

symmetrically on two sides of the localization belt in the upper, middle and lower parts, respectively. Figure 6 shows the relationship curves of tension-induced displacement and stress over time at the measuring points in the representative rock samples. It is easy to see that the tension-induced displacement is the largest in the medium sandstone, followed by the fine sandstone, sandy mudstone and siltstone successively.

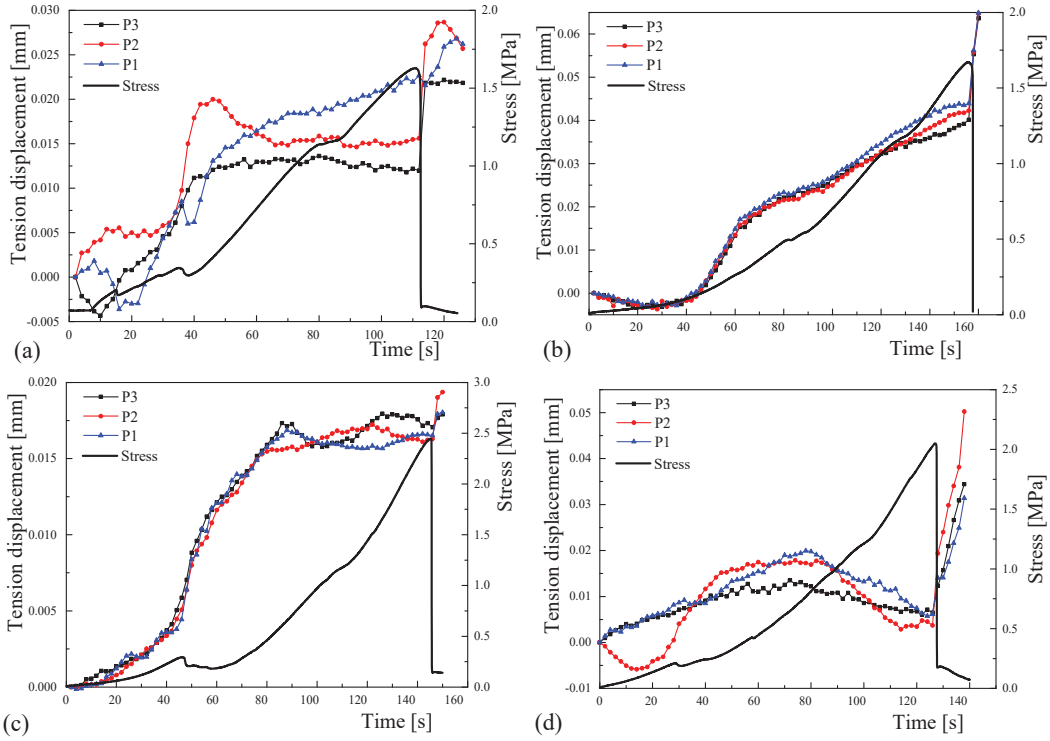

Figure 6. Relationship curves of tension-induced displacement and stress over time at each measuring point in different rock samples; (a) sandy mudstone sample 022, (b) medium sandstone sample 411, (c) siltstone sample 516, and (d) fine sandstone sample 531

As shown in fig. 6, there are some differences in tension-induced displacement at different measuring points of the sandy mudstone sample 022 during the compaction stage, whereas the variation of tension-induced displacement is basically consistent at each measuring point in the medium sandstone sample 411, 516, and 531. It is because sample 022 has more anisotropic.

The AE features of weakly cemented rocks

The AE signal monitoring is a good method to understand crack initiation, propagation and penetration inside the coal rocks. The *R* value of AE (ratio of cumulative AE count to cumulative energy) can reflect the situation of crack propagation inside the rock specimens. Figure 7 shows the curves of cumulative AE energy and *R* value over time. The *R* value first increases and then decreases in the sandy mudstone sample 022 during the compaction stage. The cracks inside the samples are compacted with damage of some structures and an increase in *R* value in the early loading phase. Then the micro-cracks propagate and low energy events occur, leading to a reduction in *R* value. During the elastic stage and the post-elastic stage, the *R* value increases slowly. There is a sudden decrease in *R* value when the stress approaches the peak strength, and the R value stabilizes in the post-peak stage.

As shown in fig. 7, there is considerable difference in cumulative AE energy in four types of rock specimens. It is the maximum in the siltstone and minimum in the fine sandstone. A sudden increase was observed in all samples before reaching the peak strength, though the increase amplitude differed significantly. The increase amplitude is the largest in the fine sandstone sample 531, which is 86.7%, and AE events decreases significantly in the compaction

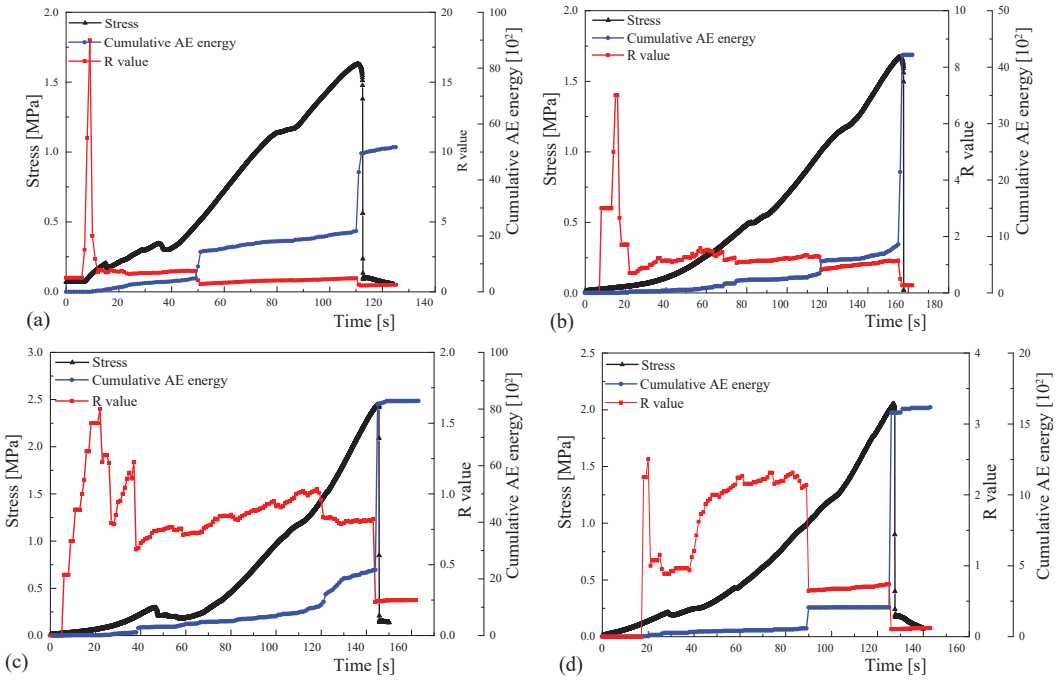

Figure 7. Relationship curves of cumulative AE energy, *R* value and stress at the measuring points in different rock samples with time; (a) sandy mudstone sample 022, (b) medium sandstone sample 411, (c) siltstone sample 516, and (d) fine sandstone sample 531

stage and elastic stage. A step-like increase occurs at 47.6% of the peak strength, while the *R* value decreases abruptly, indicating the occurrence of high energy AE events and considerable structural damage. The increase amplitude of cumulative AE energy is the smallest in sandy mudstone sample 022, which is 57.1%. The cumulative AE energy increases continuously during the entire process, with a step-like increase at 28.8% of peak strength, while the *R* value decreases suddenly.

Taken together, the evolution of *R* value during the splitting failure process in four types of rock samples is basically consistent. During the compaction stage, the *R* value first increases and then decreases. That is probably due to the different contents in the rock samples. During the elastic stage, the *R* value increases in a fluctuating manner until a sudden decrease in the late elastic stage. In the post-elastic stage, the *R* value basically remains stable until a sudden decrease when approaching the peak strength. A relatively stable trend is maintained in the post-peak stage.

Conclusion

In our work, the basically consistent evolution of tension-induced displacement in four types of the rock samples during the entire deformation failure process was considered. In the compaction stage, the anisotropy leads to different displacement at different measuring points. The displacement increases slowly in the elastic stage and post-elastic stage. When the stress approaches the peak strength, there is a sudden increase in the displacement, which serves as a precursory feature for splitting failure in rock samples. The evolution rule of *R* value is basically consistent in four types of rock samples. During the compaction stage, the *R* value first increases and then decreases due to the different contents of minerals. The *R* value increases in a fluctuating manner until a sudden decrease in the late elastic stage; The *R* value basically remains stable until a sudden decrease when approaching the peak strength. A relatively stable trend maintains in the post-peak stage.

Acknowledgment

The authors are grateful to the financial support from National Natural Science Foundation of China (51874312, U1910206), the YueQi Distinguished Scholar Project of China University of Mining & Technology-Beijing, the Open Fund of Key Laboratory of Safety and High-efficiency Coal Mining (JYBSYS2019101), the Fundamental Research Funds for the Central Universities (2020YQNY07) and National Training Program of Innovation and Entrepreneurship for Undergraduates (C201911370, C202011039), and State Key Laboratory of Water Resources Protection and Utilization in Coal Mining independent Research Project (GJNY-18-77).

References

[1] Li, H., *et al.*, Physical and Mechanical Characteristics and Definition of Weakly Cemented Sandstone (in Chinese), *Coal Science and Technology*, *45* (2017), pp. 1-7
[2] Li, H., *et al.*, Mechanical Properties and Acoustic Emission Characteristics of Thick Hard Roof Sandstone in Shendong Coal Field, *International Journal of Coal Science and Technology*, *4* (2017), Mar., pp. 147-158
[3] Wang, Z., *et al.*, Relationships Between the Petrographic, Physical and Mechanical Characteristics of Sedimentary Rocks in Jurassic Weakly Cemented Strata, *Environmental Earth Sciences*, *78* (2019), Feb., pp. 131
[4] Wang, H., *et al.*, Experimental Study on Fracture Process of Sintered Nd-Fe-B Magnets During Dynamic Brazilian Tests, *Journal of Magnetism and Magnetic Materials*, *471* (2019), Feb., pp. 200-208

[5] Sanborn, B., *et al.*, Revisit of Dynamic Brazilian Tests of Geomaterials, in: *Dynamic Behavior of Material*, Springer, New York, USA, Vol. 1, pp. 143-145
[6] Yang, S. Q., *et al.*, Experiment and Discrete Element Modelling on Strength, Deformation and Failure Behaviour of Shale under Brazilian Compression, *Rock Mechanics and Rock Engineering*, *52* (2019), May, pp. 4339-4359
[7] Suchorzewski, J., *et al.*, Experimental and Numerical Investigations of Concrete Behaviour at Meso-Level During Quasi-Static Splitting Tension, *Theoretical and Applied Fracture Mechanics*, *96* (2018), Aug., pp. 720-739
[8] Aliabadian, Z., *et al.*, Crack Development in Transversely Isotropic Sandstone Discs Subjected to Brazilian Tests Observed Using Digital Image Correlation, *International Journal of Rock Mechanics and Mining Sciences*, *119* (2019), July, pp. 211-221
[9] Fan, G., *et al.*, Experimental Study on the Permeability of Weakly Cemented Rock under Different Stress States in Triaxial Compression Tests, *Geofluids*, *2018* (2018), ID 9035654
[10] Labuz, J. F., *et al.*, Acoustic Emission at Failure in Quasi-Brittle Materials, *Construction and Building Materials*, *15* (2001), 5-6, pp. 225-233
[11] Wang, H., *et al.*, Experimental Study on Acoustic Emission of Weakly Cemented Sandstone Considering Bedding Angle, *Shock and Vibration*, *2018* (2018), ID 6086583
[12] Liu, H., *et al.*, Behavior of Weakly Cemented Rock with Different Moisture Contents under Various Tri-Axial Loading States, *Energies*, *12* (2019), 8, pp. 1-15
[13] Zhao, Y., *et al.*, Dynamic Tensile Strength of Coal under Dry and Saturated Conditions, *Rock Mechanics and Rock Engineering*, *49* (2016), Sept., pp. 1709-1720
[14] Byun, Y. S., *et al.*, A Study on Using Acoustic Emission in Rock Slope with Difficult Ground-Focused on Rainfall, *Geosciences Journal*, *16* (2012), Dec., pp. 435-445
[15] Wang, J., *et al.*, Effect of Layer Orientation on Acoustic Emission Characteristics of Anisotropic Shale in Brazilian Tests, *Journal of Natural Gas Science and Engineering*, *36* (2016), Part B, pp. 1120-1129

Paper submitted: May 29, 2020
Paper revised: August 15, 2020
Paper accepted: August 30, 2020